



La Science à l'œuvre pour le  
at work for Canada

## NRC Publications Archive (NPArc) Archives des publications du CNRC (NPArc)

### **Effect of aggregation on the absorption cross-section of fractal soot aggregates and its impact on LII modelling**

Liu, Fengshan; Smallwood, Gregory J.

#### **Publisher's version / la version de l'éditeur:**

*Journal of Quantitative Spectroscopy and Radiative Transfer*, 111, 2, pp. 302-308, 2010-01-01

#### **Web page / page Web**

<http://dx.doi.org/10.1016/j.jqsrt.2009.06.017>

<http://nparc.cisti-icist.nrc-cnrc.gc.ca/npsi/ctrl?action=rtdoc&an=15195100&lang=en>

<http://nparc.cisti-icist.nrc-cnrc.gc.ca/npsi/ctrl?action=rtdoc&an=15195100&lang=fr>

Access and use of this website and the material on it are subject to the Terms and Conditions set forth at

[http://nparc.cisti-icist.nrc-cnrc.gc.ca/npsi/jsp/nparc\\_cp.jsp?lang=en](http://nparc.cisti-icist.nrc-cnrc.gc.ca/npsi/jsp/nparc_cp.jsp?lang=en)

READ THESE TERMS AND CONDITIONS CAREFULLY BEFORE USING THIS WEBSITE.

L'accès à ce site Web et l'utilisation de son contenu sont assujettis aux conditions présentées dans le site

[http://nparc.cisti-icist.nrc-cnrc.gc.ca/npsi/jsp/nparc\\_cp.jsp?lang=fr](http://nparc.cisti-icist.nrc-cnrc.gc.ca/npsi/jsp/nparc_cp.jsp?lang=fr)

LISEZ CES CONDITIONS ATTENTIVEMENT AVANT D'UTILISER CE SITE WEB.

Contact us / Contactez nous: [nparc.cisti@nrc-cnrc.gc.ca](mailto:nparc.cisti@nrc-cnrc.gc.ca).



National Research  
Council Canada

Conseil national  
de recherches Canada

Canada



Contents lists available at ScienceDirect

# Journal of Quantitative Spectroscopy & Radiative Transfer

journal homepage: [www.elsevier.com/locate/jqsrt](http://www.elsevier.com/locate/jqsrt)

## Effect of aggregation on the absorption cross-section of fractal soot aggregates and its impact on LII modelling

Fengshan Liu\*, Gregory J. Smallwood

Institute for Chemical Process and Environmental Technology, National Research Council, Building M-9, 1200 Montreal Road, Ottawa, Ontario, Canada K1A 0R6

### ARTICLE INFO

#### Article history:

Received 12 June 2009

Accepted 23 June 2009

#### Keywords:

Fractal soot aggregates

Absorption cross-section

Laser-induced incandescence

### ABSTRACT

This study concerns the effect of particle aggregation on laser heating rate of soot aggregates in laser-induced incandescence. Three aggregate absorption models were investigated: the Rayleigh–Debye–Gans approximation, the electrostatics approximation, and the numerically exact generalized multi-sphere Mie-solution method. Fractal aggregates containing 5–893 primary particles of 30 nm in diameter were generated numerically using a combined particle-cluster and cluster-cluster aggregation algorithm with specific fractal parameters typical of soot. The primary particle size parameters considered are 0.089, 0.177, and 0.354. The Rayleigh–Debye–Gans approximation neglects the effect of particle aggregation on absorption; so it underestimates the aggregate absorption cross-section area by approximately 10%, depending on the aggregate size and primary particle size parameter. The electrostatics approximation is somewhat better than the Rayleigh–Debye–Gans approximation, but cannot account for the effect of primary particle size parameter. The aggregate absorption submodel affects the calculated soot temperature in laser-induced incandescence mainly in the low laser fluence regime. At high laser fluences, the effect diminishes due to the enhanced importance of soot sublimation cooling and neglect of aggregation effect in the sublimation in the present numerical model of laser-induced incandescence.

Crown Copyright © 2009 Published by Elsevier Ltd. All rights reserved.

### 1. Introduction

It has been established that combustion-generated soot appears as fractal aggregates formed by nearly spherical primary particles of more or less the same size. The structure of fractal aggregates is rather complex and appears like grape clusters with significant proportion of space between the branches. In diffusion flames the aggregate size (the number of primary particles within aggregate) can vary from a few to several hundreds or even thousands. The structure of an individual fractal aggregate formed by identical primary particles can be described statistically by the scaling relationship among

the number of primary particles  $N$ , the radius of gyration  $R_g$ , and the radius of primary particle  $a$  [1]. The complex and fairly open geometry of such fractal aggregates cannot be represented by a compact sphere. Consequently, the radiative properties of soot cannot be described by either the Mie theory or the Rayleigh approximation [2,3].

The absorption cross-section is one of the fundamental radiative properties of soot fractal aggregates. Such knowledge is not only important for accurate evaluation of the contribution of soot to thermal radiation transfer in flames, fires, and combustion systems, but is also required in many absorption- and emission-based diagnostic techniques for soot measurements (volume fraction and primary particle size). For example, the absorption cross-section of soot aggregates is required to calculate the laser energy absorption rate and the thermal radiation intensity in laser-induced incandescence (LII) techniques when the

\* Corresponding author.

E-mail address: [Fengshan.liu@nrc-cnrc.gc.ca](mailto:Fengshan.liu@nrc-cnrc.gc.ca) (F. Liu).

Nomenclature			
$a$	primary particle radius	$R$	correction factor
$C_a$	aggregate absorption cross-section	$R_g$	radius of gyration
$c$	specific heat	$R_u$	universal gas constant
$D_f$	fractal dimension	$T$	soot temperature
$d$	diameter	$t$	time
$F_0$	laser fluence at 1 m]	$x_p$	size parameter
$k$	imaginary part of the refractive index	<i>Greek symbols</i>	
$k_f$	fractal prefactor	$\beta$	effective sublimation coefficient
$M$	molecular weight	$\rho$	density
$m$	refractive index	$\lambda$	wavelength
$n$	real part of the refractive index	$\Delta H$	heat of sublimation
$N$	number of primary particle in aggregate	<i>Subscripts</i>	
$q$	laser power density	p	particle
$q_c$	conduction loss rate	s	soot
$q_r$	radiation loss rate		

effect of soot particle aggregation is taken into account [4,5]. Although aggregation of primary particles could potentially affect the ability of soot to absorb and emit light, it has been neglected in the context of the popular Rayleigh–Debye–Gans (RDG) approximation [6]. The accuracy of the RDG approximation has been extensively validated using various more accurate methods. It is generally agreed that in the visible spectrum RDG underestimates the absorption cross-section of soot fractal aggregates by about 10% for typical primary particles of 30 nm in diameter. Although such level of error may be considered acceptable in some applications, such as laser extinction, it becomes unacceptable in low-fluence LII applications [7]. Therefore, a more accurate model for the absorption cross-section of soot is required to model LII.

Due to the fact that soot appears as fractal aggregates rather than isolated primary particles, incorporation of the aggregation effect into LII models has become an active research area. The effect of particle aggregation on heat conduction cooling of soot particles, which is important after laser pulse, has been investigated by Liu et al. [4,5]. In those studies, however, the effect of particle aggregation on the laser energy absorption term was neglected based on the RDG approximation. The study of this effect is very important to the further development of aggregate-based LII models. The objectives of this study are twofold: (1) to quantify the effect of aggregation on the absorption property of soot aggregates using three models of different accuracies: the RDG approximation [6], the electrostatics approximation (ESA) [8], and the generalized multi-sphere Mie-solution (GMM) method [9–11] and (2) to investigate how soot temperature is affected by different soot aggregate absorption submodels in LII modelling.

## 2. Methodology

The methodology used in this study to evaluate the accuracy of the RDG and the ESA (and several other ones)

offers the following advantages compared with previous similar studies. First, the algorithm for the generation of fractal aggregates ensures that the fractal scaling relationship is always satisfied. All the numerically generated aggregates have identical prefactors and fractal dimensions. Consequently, the present results of the soot absorption cross-sections are not contaminated by variation in fractal parameters from one aggregate size to the other. Secondly, GMM is a numerically exact method that provides more accurate results than the less accurate techniques such as RDG, ESA, and several others, used in previous studies.

### 2.1. Numerical generation of fractal aggregates

To simplify the problem but also reasonably represent real soot aggregates it is commonly assumed that primary particles within any given aggregate are identical and in point touch. The fractal-like structure of soot aggregates obey the following statistical scaling law [1]:

$$N = k_f \left( \frac{R_g}{a} \right)^{D_f} \quad (1)$$

The radius of gyration  $R_g$  is defined as [12]

$$R_g^2 = \frac{1}{N} \sum_{i=1}^N (\mathbf{r}_i - \mathbf{r}^0)^2 + a^2 \quad (2)$$

$$\mathbf{r}^0 = \frac{1}{N} \sum_{i=1}^N \mathbf{r}_i \quad (3)$$

where vectors  $\mathbf{r}_i$  and  $\mathbf{r}^0$  define the position of the  $i$ th primary particle centre and the centre of the aggregate, respectively. In this study, fractal aggregates simulating flame-generated soot were numerically generated using the particle-cluster aggregation algorithm for small aggregates (up to  $N = 31$ ) and cluster-cluster aggregation algorithm for larger aggregates. The algorithms used in this study follow closely those described by Filippov et al. [12] and the details of our numerical implementation of

these algorithms can be found in [13]. The following morphological parameters were used in the generation of fractal aggregates:  $k_f = 2.3$ ,  $D_f = 1.78$ , and  $a = 15$  nm, which are typical values for flame-generated soot. Fractal aggregates containing 5–893 primary particles were generated using this combined particle-cluster and cluster-cluster aggregation algorithm.

## 2.2. Generalized multi-sphere Mie solution

GMM was used to calculate the orientation-averaged radiative properties of the numerically generated fractal aggregates to represent those of a random-oriented ensemble of soot aggregates. Similar to the superposition  $T$ -matrix method [14], GMM is also numerically exact and much more efficient than other numerical techniques based on an explicit solution of the Maxwell equations. GMM was developed by Xu [9,10] based on the framework of the Mie theory for a single sphere and the addition theorems for spherical vector wave functions. GMM provides rigorous and complete solution to non-overlapping multi-sphere light scattering problems and can be readily applied to fractal aggregates [13,15]. Execution of this numerically exact method requires the positions, diameter, and refractive index of each constituent sphere (primary particle). Although  $T$ -matrix has become the most popular method to study the radiative properties of various scatterers [16], GMM has also been demonstrated to be a powerful tool to study radiative properties of various particles [9,10,13,15]. In fact,  $T$ -matrix and GMM share a very similar theoretical framework, though differences exist [11]. GMM offers some advantages over the  $T$ -matrix method, as discussed by Xu and Khlebtsov [11]. The key steps involved in the development of GMM include: (a) expansion of the scattered, internal, and incident electromagnetic fields in terms of vector spherical functions, (b) formation of a linear equation system through the boundary condition at each primary particle in the aggregate, (c) transformation of the waves scattered by an individual primary particle into the incident waves of the other particles in the aggregate through the addition theorems for vector spherical functions, and (d) solution of the linear system of interactive coefficients. GMM rigorously accounts for the multiple scattering within the aggregate. However, GMM is computationally very demanding and memory intensive for large aggregates containing several hundreds of primary particles, especially when the size parameter of primary particle is large (on the order of 1 or larger).

Although most of the GMM results were obtained for a single aggregate realization, the effect of realization averaging was also investigated by generating 10 different aggregates of identical morphology for  $N = 10$ –800. However, such calculations were conducted only for  $\lambda = 532$  nm. The corresponding primary particle size parameter  $(\pi d_p/\lambda)x_p$  is relatively small (0.177).

## 3. LII model

The following aggregate-based LII model was used for the purpose of demonstrating the effect of aggregation on

laser energy absorption rate of soot aggregate in such application. It is formulated in terms of energy and mass conservation equations as [5,7]

$$\frac{1}{6} \pi d_p^3 N \rho_s c_s \frac{dT}{dt} = C_a F_0 q(t) - q_c - q_r + N \frac{\Delta H_v}{M_v} \frac{dM}{dt} \quad (4)$$

$$\frac{dM}{dt} = \frac{1}{2} \rho_s \pi d_p^2 \frac{dd_p}{dt} = -\pi d_p^2 \beta p_v \sqrt{\frac{M_v}{2\pi R_u T}} \quad (5)$$

The effective sublimation coefficient  $\beta$  was chosen as 0.9. Soot aggregate heat loss after the laser pulse due to radiation,  $q_r$ , and conduction,  $q_c$ , were calculated using the expressions given in [5]. Note that the effect of aggregation on heat conduction was taken into account as described in [5]. It is implicitly assumed in Eq. (4) that any potential temperature non-uniformity among primary particles within an aggregate is neglected. The effect of aggregation on thermal radiation loss from soot aggregate is neglected, since radiation loss is negligible compared to heat loss due to sublimation or conduction under the present conditions. It is also worth pointing out that the effect of aggregation on soot sublimation, the last term on the right hand side of Eq. (4), was completely neglected due to lack of better knowledge currently.

Three aggregate absorption cross-section models are considered in this work. The first one is that from the numerical results of GMM calculations for the numerically generated soot fractal aggregates. Such absorption cross-sections are considered numerically exact. The second one is the RDG approximation. In this approximate theory, multiple scattering is neglected and the interactions between primary particles are absent as far as absorption is concerned. The aggregate absorption cross-section can then be written as [5,6]

$$C_a = N C_a^p = N \frac{\pi^2 d_p^3 E(m)}{\lambda} \quad (6)$$

where  $E(m) = \text{Im}[(m^2-1)/(m^2+2)]$  is the soot absorption function and  $C_a^p$  is the absorption cross-section of a primary particle in the Rayleigh regime. The third aggregate absorption cross-section model is the electrostatics approximation [8]. In ESA, it is assumed that all characteristic lengths of the aggregate are significantly smaller than the wavelength. Although this assumption is reasonable for primary particles in the visible and near infrared, it is highly questionable for relatively large aggregates in these spectrum regions. A simple expression for the aggregate absorption cross-section in ESA has been developed by Mackowski [8] as

$$C_a = N C_a^p R(N, m) \quad (7)$$

where the correction factor  $R$  is a function of aggregate size and soot refractive index and is given as

$$R(N, m) = 1 + [R_{\text{abs},\infty}(m) - 1] \left(1 - \frac{3}{2N+1}\right) \quad (8)$$

$$R_{\text{abs},\infty}(m) = \frac{1}{\text{Im}f_1} \sum_{i=1}^{10} c_i \text{Im}(f_1)^i \quad (9)$$

where  $f_1$  is given as  $f_1 = (m^2 - 1)/(m^2 + 2)$ . The expansion coefficients  $c_i$  are given in [8].

#### 4. Results and discussion

GMM calculations were conducted for 1064, 532, and 266 nm wavelengths, since 1064 and 532 nm are the most common laser wavelengths used to excite soot in LII experiments. A shorter wavelength of 266 nm was also investigated to achieve a higher primary particle size parameter. The corresponding primary particle size parameters are relatively small at 0.0886, 0.177, and 0.354, respectively. The refractive index of soot was assumed to be  $m = 1.6 + 0.6i$ , which is again a typical value for soot in the visible spectrum. Orientation averaging was achieved numerically in the GMM calculations by dividing each Euler angle into at least 10 equal intervals. Such a level of orientation averaging was found to be sufficient, i.e., further division of the three Euler angles did not affect the orientation-averaged results.

##### 4.1. Absorption cross-section of soot aggregates

The nondimensional absorption cross-sections of soot aggregates calculated from the three models are compared in Fig. 1. For RDG approximation, the nondimensional absorption cross-section remains at unity for any aggregate sizes, i.e., the effect of aggregation on aggregate absorption is completely absent. Although ESA is somewhat superior to RDG and captures some qualitative features of the effect of aggregation on absorption, i.e., aggregation enhances the ability of aggregates to absorb light, it fails in the following two aspects. First, it predicts an increase in the absorption cross-section with increasing aggregate size  $N$  and then reaches a plateau. GMM, on the other hand, predicts that the absorption cross-section first increases and then decreases. Secondly, ESA could not account for the effect of primary particle size parameter. GMM results show that the primary particle size parameter (achieved here by varying the wavelength) has a

significant influence on the absorption cross-section, not only the magnitude but also the overall variation trend with  $N$ . Results of ESA are in reasonable agreement with those of GMM for the smallest size parameter. The agreement between ESA and GMM deteriorates as  $x_p$  increases. This is expected given the assumption made in the ESA formulation [8]. It is clear that neither RDG nor ESA can accurately predict the aggregate absorption cross-sections.

Although the variation of the absorption cross-section with aggregate size  $N$  is more pronounced with increasing  $x_p$ , all three GMM curves exhibit the same overall trend. The absorption cross-section first increases with increasing  $N$  to reach a peak value at a certain  $N$  and then starts to decrease at larger  $N$ . The present GMM results, however, are superior to previous numerical studies in terms of the consistency of the fractal properties from aggregate to aggregate and the accuracy of the solution method [13]. The enhanced absorption for relatively small aggregates is attributed to the coupling between electric fields of primary particles or the multiple scattering effect [17,18]. For even larger aggregates, the shielding effect, which reduces the absorption ability of the aggregate, becomes increasingly important and eventually results in the decrease in the absorption cross-section. Such shielding effect can be observed either at large aggregate sizes for a given primary particle size parameter as shown in Fig. 1 and the results of Mulholland and Mountain [17] or at large primary particle size parameter for a given aggregate size [18]. The net effect of coupling and shielding is controlled by the relative importance of these two competing factors.

It is also noticed that for  $N = 1$  (single primary particle), both RDG and ESA yield unity nondimensional absorption cross-section as expected. However, results of GMM at  $N = 1$  depart from unity even at relatively small  $x_p$  ( $> \sim 0.1$ ) due to the fact that GMM provides Mie solutions instead of Rayleigh ones for a spherical particle.

The curve with dark grey circles in Fig. 1 represents results after realization averaging for  $\lambda = 532$  nm, i.e.,  $x_p = 0.177$ . These results indicate that the effect of realization averaging is quite small. Therefore, the orientation-averaged absorption cross-sections obtained from a single realization can be used to represent those of a random-oriented ensemble of fractal aggregates. This observation is in agreement with that made by Liu and Mishchenko [19].

##### 4.2. Effect of absorption model on LII modelling

Calculations of the temporal evolution of soot temperature and primary particle diameter were carried out using the three aggregate absorption submodels discussed above for a laser wavelength of 532 nm. Except the value of  $\beta$  (0.9) and the soot absorption function  $E(m)$  at 532 nm, all other model parameters, including the laser temporal power density  $q(t)$ , were taken from previous studies [4,7]. For the assumed soot refractive index in the visible,  $m = 1.6 + 0.6i$ , the corresponding  $E(m)$  is 0.27. The ambient

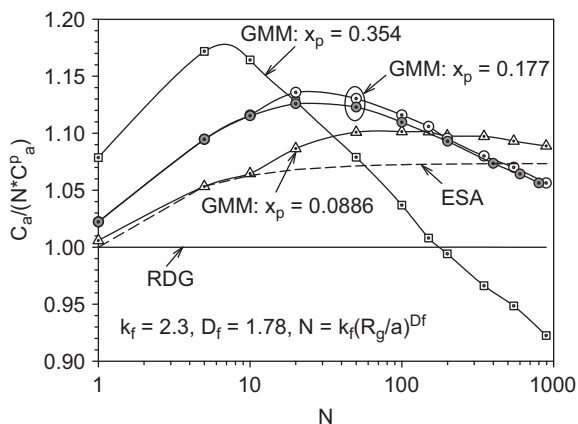


Fig. 1. Nondimensional absorption cross-sections predicted by GMM, ESA, and RDG. The open circles represent results of GMM for single aggregate realization. The filled circles are realization-averaged GMM results.

pressure and temperature are 1 atm and 1700 K, respectively.

The predicted soot temperature histories using the three aggregate absorption submodels for four different aggregate sizes are compared in Fig. 2 at a low laser fluence of  $0.65 \text{ mJ/mm}^2$ . Use of RDG approximation results in nearly identical peak soot temperature, i.e., independent of aggregate size  $N$ , and temperature decays slower with increasing  $N$ , Fig. 2(a). The slower temperature decay for a larger aggregate is the result of shielding effect for heat conduction [4,5]. The effect of aggregation has a large impact on the peak soot temperature as indicated by the GMM results, Fig. 2(a). The peak soot temperature predicted by the GMM absorption submodel exhibits a relatively large dependence on the aggregate size. The maximum peak soot temperature among the four aggregates is reached at 3407.6 K for  $N = 10$ , which is 160 K higher than that predicted by the RDG approximation. The peak soot temperature for  $N = 100$  is almost identical to that of  $N = 10$ . The peak soot temperature for  $N = 500$  is slightly lower than that for  $N = 100$ , reflecting the fact that the GMM absorption cross-sections for  $x_p = 0.177$  ( $\lambda = 532 \text{ nm}$ ) decrease with increasing  $N$  for  $N > 20$ , Fig. 1. However, it is interesting to observe that the soot temperature decay for  $N = 500$  is actually slower than that for  $N = 100$  at long times when  $t > 100 \text{ ns}$ , Fig. 2(a). This is attributed to the following two factors. First, the higher peak temperature for  $N = 100$  leads to slightly greater sublimation cooling rate around the end of the laser pulse ( $\sim 25 \text{ ns}$ ). However, this factor is believed to be very minor at such relatively low temperatures. Secondly, the effective diameter for heat conduction for  $N = 100$  is smaller than that for  $N = 500$  [4,5]. This is the main reason for the faster temperature decay for  $N = 100$ .

Overall, the ESA absorption submodel performs better than RDG in terms of the peak soot temperatures and the temperature decay rate, Fig. 2(b). Unlike RDG, which fails

to predict the effect of aggregation on the peak soot temperature, ESA is partially capable of predicting the effect of aggregation on soot temperature, but does not predict the full increase displayed by the GMM results.

The predicted soot temperature histories at a higher laser fluence of  $F_0 = 1.5 \text{ mJ/mm}^2$  are compared in Fig. 3. It is somewhat surprising to observe that at this relatively high laser fluence different treatments for the aggregate absorption have only a small impact on the peak soot temperature and negligible impact on soot temperatures right after the peak. Examination of the numerical results indicates that the peak soot temperatures (reached around  $t = 13 \text{ ns}$ ) predicted by the three absorption submodels for  $N = 1\text{--}500$  differ by less than 66 K. At  $t = 400 \text{ ns}$ , soot temperatures of different aggregate sizes display somewhat larger differences. However, for a given aggregate size the soot temperatures predicted by the three absorption submodels differ by less than 7 K at  $t = 400 \text{ ns}$ . These observations can be explained as follows. The smaller deviations among the peak soot temperature of different aggregate sizes and different absorption submodels are caused by the enhanced soot sublimation cooling, which is significant around 4250 K. At low laser fluences, the peak soot temperature is mainly governed by the balance between the internal energy variation rate and the laser heating rate, since heat conduction cooling rate is small compared to laser heating. At high laser fluences, however, the peak soot temperature is also affected by sublimation cooling, which is very high and hence somewhat diminishes the differences in the laser heating rate due to different absorption submodels. Between shortly after the peak temperature and about 50 ns, soot temperatures of different aggregates sizes calculated by different absorption submodels are essentially identical. It is recognized that these results should be viewed with caution since the effect of aggregation on the soot aggregate sublimation process is neglected, see the sublimation term in Eq. (1). At longer times (after  $\sim 50 \text{ ns}$ ), soot temperatures

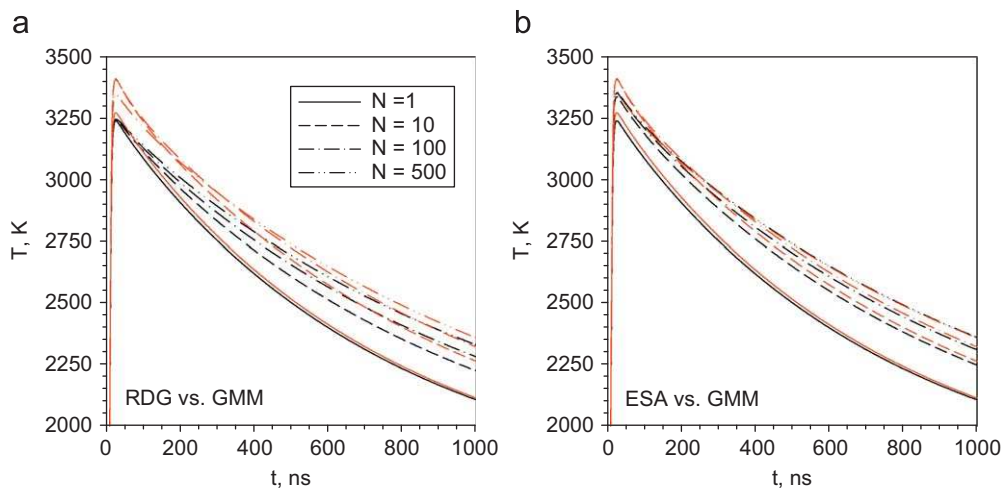
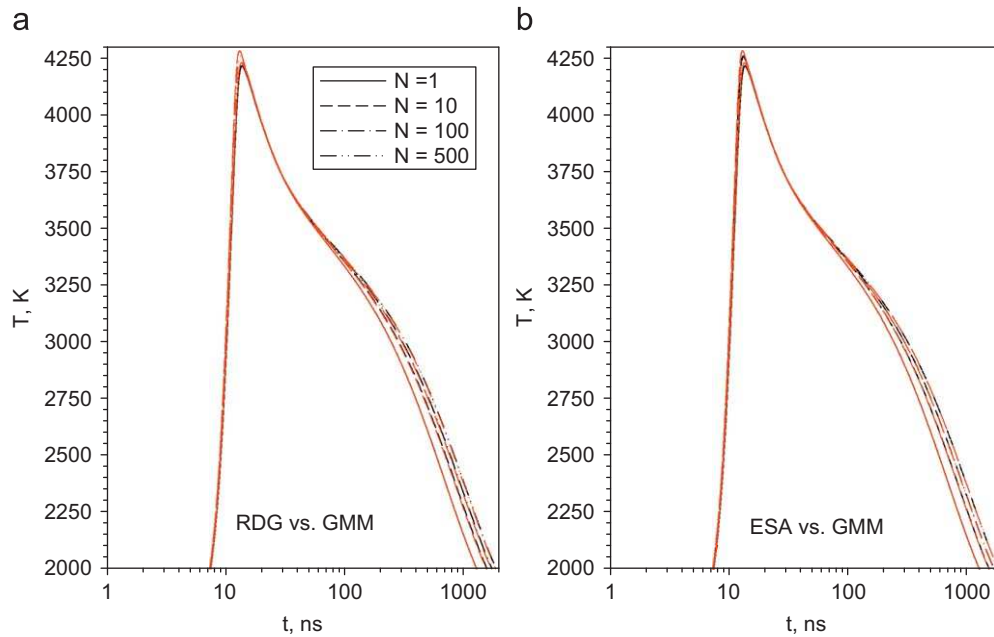


Fig. 2. Soot temperature histories predicted by three aggregate absorption submodels for  $F_0 = 0.65 \text{ mJ/mm}^2$ . Black lines are either RDG (a) or ESA (b). Red lines are GMM. (For interpretation of the references to colour in this figure legend, the reader is referred to the web version of this article.)



**Fig. 3.** Soot temperature histories predicted by three aggregate absorption submodels for  $F_0 = 1.5 \text{ mJ/mm}^2$ . See Fig. 2 for legends. (For interpretation of the references to colour in this figure legend, the reader is referred to the web version of this article.)

of different aggregate sizes deviate from one another, reflecting the effect of aggregation on heat conduction cooling.

## 5. Conclusions

Results of the numerically exact GMM method show that aggregation affects the ability of soot aggregate to absorb light. It can either enhance or decrease its absorption cross-section, depending on the relative importance of electric field coupling and the shielding effect among primary particles, which is in turn determined by the aggregate size and the primary particle size parameter. The RDG theory completely neglects the effect of aggregation on absorption. The ESA can only partially account for the effect of aggregation on absorption; however, it cannot account for the effect of primary particle size parameter, which is rather significant. Effect of aggregation on aggregate laser energy absorption was found to be significant in LII modelling in the low laser fluence regime. Such an effect, however, was found to be unimportant at high laser fluences. This finding must be viewed with caution due to the neglect of aggregation impact on sublimation. Further study is required to investigate the effect of particle aggregation on LII modelling for polydisperse fractal soot aggregates and the effect of aggregation on soot sublimation.

## References

- [1] Forrest SR, Witten Jr TA. Long-range correlations in smoke-particle aggregates. *J Phys A: Math Gen* 1979;12:L109–17.
- [2] Dalzell WH, Williams GC, Hottel HC. A light-scattering method for soot concentration measurements. *Combust Flame* 1970;14:161–70.
- [3] Köylü ÜÖ, Faeth GM. Radiative properties of flame-generated soot. *J Heat Transfer* 1993;115:409–17.
- [4] Liu F, Smallwood GJ, Snelling DR. Effects of primary particle diameter and aggregate size distribution on the temperature of soot particles heated by pulsed lasers. *J Quant Spectrosc Radiat Transfer* 2005;93:301–12.
- [5] Liu F, Yang M, Hill FA, Snelling DR, Smallwood GJ. Influence of polydisperse distributions of both primary particle and aggregate size on soot temperature in low-fluence LII. *Appl Phys B* 2006;83:383–95.
- [6] Köylü ÜÖ, Faeth GM. Optical properties of overfire soot in buoyant turbulent diffusion flames at long residence time. *J Heat Transfer* 1994;116:152–9.
- [7] Liu F, Daun KJ, Beyer V, Smallwood GJ, Greenhalgh DA. Some theoretical considerations in modelling laser-induced incandescence at low-pressures. *Appl Phys B* 2007;87:179–91.
- [8] Mackowski DW. A simplified model to predict the effects of aggregation on the absorption properties of soot particles. *J Quant Spectrosc Radiat Transfer* 2006;100:237–49.
- [9] Xu Y-L. Electromagnetic scattering by an aggregate of spheres. *Appl Opt* 1995;34:4573–88.
- [10] Xu Y-L. Electromagnetic scattering by an aggregate of spheres: far field. *Appl Opt* 1997;36:9496–508.
- [11] Xu Y-L, Khlebtsov NG. Orientational-averaged radiative properties of an arbitrary configuration of scatterers. *J Quant Spectrosc Radiat Transfer* 2003;79–80:1121–37.
- [12] Filippov AV, Zurit M, Rosner DE. Fractal-like aggregates: relation between morphology and physical properties. *J Colloid Interface Sci* 2000;229:261–73.
- [13] Liu F, Snelling DR. Evaluation of the accuracy of the RDG approximation for the absorption and scattering properties of fractal aggregates of flame-generated soot. *AIAA-2008-4362*, 2008.
- [14] Mishchenko MI. Light scattering by randomly oriented axially symmetric particles. *J Opt Soc Am A* 1991;8:871–82.
- [15] Van-Hulle P, Weill M-E, Talbaut M, Coppalle A. Comparison of numerical studies characterizing optical properties of soot aggregates for improved EXSCA measurements, part. *Part Syst Charact* 2002;19:47–57.

- [16] Mishchenko MI, Videen G, Khlebtsov G, Wriedt T, Zakharova NT. Comprehensive *T*-matrix reference database: a 2006–07 update. *J Quant Spectrosc Radiat Transfer* 2008;109:1447–60.
- [17] Mulholland GW, Mountain RD. Coupled dipole calculation of extinction coefficient and polarised ratio for smoke agglomerates. *Combust Flame* 1999;119:56–68.
- [18] Mulholland GW, Bohren CF, Fuller KA. Light scattering by agglomerates: coupled electric and magnetic dipole method. *Langmuir* 1994;10:2533–46.
- [19] Liu L, Mishchenko MI. Scattering and radiative properties of complex soot and soot-containing aggregate particles. *J Quant Spectrosc Radiat Transfer* 2007;106:262–73.